Density functional theory simulations of B K and N K NEXAFS spectra of h-BN/transition metal(111) interfaces

2009 J. Phys.: Condens. Matter 21 104210

(http://iopscience.iop.org/0953-8984/21/10/104210)

IOP PUBLISHING JOURNAL OF PHYSICS: CONDENSED MATTER

J. Phys.: Condens. Matter **21** (2009) 104210 (8pp) doi:10.1088/0953-8984/21/10/104210

Density functional theory simulations of B K and N K NEXAFS spectra of h-BN/transition metal(111) interfaces

R Laskowski, Th Gallauner, P Blaha and K Schwarz

Vienna University of Technology, A-1060 Vienna, Austria

Received 4 September 2008, in final form 24 October 2008
Published 10 February 2009
Online at stacks.iop.org/JPhysCM/21/104210

Abstract

The electronic structure and the corresponding B K and N K near-edge x-ray fine structure (NEXAFS) spectra of epitaxially grown h-BN on Ni(111), Pt(111), and Rh(111) surfaces are investigated by density functional theory. The calculations are carried out using the WIEN2k program package applying the augmented-plane-wave + local orbitals (APW + lo) method. The NEXAFS spectra are simulated using a $3 \times 3 \times 1$ super cell and considering the final state rule by means of a (partial) core hole for the corresponding atom. The influence of a full or partial core hole is shown for the h-BN/Ni(111) system, for which the best agreement with the experimental spectra is found when half a core hole is assumed. All characteristic features of the experimental spectra are well reproduced by theory, including the angular dependences. The bonding effects are investigated by comparing the spectra of bulk h-BN with those of the h-BN/Ni(111) system. An analysis of both the density of states and charge densities reveals strong N-p_z–Ni-d_{z^2} bonding/antibonding interactions. In the case of Pt(111) and Rh(111) surfaces, we discuss the effects of the nanomesh structures in terms of simple 1×1 commensurate models.

(Some figures in this article are in colour only in the electronic version)

1. Introduction

Hexagonal boron nitride forms well ordered and robust monolayers on many transition metal surfaces. The successful formation of an h-BN/metal interface has been reported for Ni(111) [21], Rh(111) [5], Cu(111) [27], Pd(110) [6], Pd(111) [20], Pt(111) [28], and Ru(001) [9] surfaces. Such insulating monolayers on (magnetic) metals offer a broad field of possible applications, a reason for the increasing interest in these interfaces over the last few years. h-BN layers are usually grown on transition metal (TM) surfaces by thermal decomposition of borazine [22] ($B_3N_3H_3$) at 1000 K under high vacuum conditions. In the case of Ni(111) and Cu(111) surfaces, the lattice size of the metal substrate matches approximately the size of h-BN, and thus a commensurate 1×1 interface is formed. The geometric structure of h-BN/Ni(111) shows a small buckling of the h-BN layer, in which the boron atoms are approximately 0.1 Å closer to the metal surface than the nitrogen atoms [10, 1]. In addition it was found theoretically that a stable monolayer only forms when N sits on top of Ni and B is either in the fcc or hcp hollow site [10, 12]. Similar considerations hold for h-BN/Cu(111), but the interaction strength between h-BN and Cu is much smaller than for Ni(111). For the other TM surfaces there is a considerable lattice mismatch, which drives the formation of some kind of nanostructure. The size and symmetry of such nanostructures depends on the specific matching conditions between substrate and h-BN, but usually nanostructures with a periodicity of about 3 nm are formed. Initially the actual atomic structure of these materials was subject of some controversy, mostly due to rather poorly resolved scanning tunneling microscopy (STM) images and the large (1 eV) splitting of the BN σ-bands measured by ultraviolet photoelectron spectroscopy (UPS) [5]. In order to explain these observations, originally a partial 'double layer' model of h-BN/Rh(111) was proposed [5]. Because of the complicated structure of this interface, it was called the 'BN-nanomesh'. A few years later, however, theoretical investigations [14, 13] showed that a highly corrugated monolayer of h-BN in a 12×13 commensurate coincidence lattice (a 13×13 supercell of h-BN on top of a 12×12 supercell of Rh(111)) exhibited a very similar σ band splitting

and could also explain the observed STM images [13]. This structure is caused by a balance between repulsive forces acting on N and attractive forces acting on the B atoms. Since the strength of these forces varies with the lateral BN position with respect to the Rh substrate, the h-BN monolayer deforms (corrugates) vertically by about 0.6 Å. This theoretically predicted, highly corrugated monolayer structure was later confirmed by new STM images [3]. Now it has become clear that the actual differences between commensurate and incommensurate interfaces are not qualitative, but more quantitative in nature and originate from the differences in the h-BN-metal interactions [15].

Besides STM and UPS measurements, these interfaces have also been thoroughly investigated by B K and N K near-edge x-ray fine structure (NEXAFS) spectroscopy [26, 29, 27, 28]. In the present work we calculate and analyze the B K and N K NEXAFS spectra of commensurate h-BN/Ni(111) and incommensurate h-BN/Rh(111) and h-BN/Pt(111) interfaces by means of density functional theory (DFT) calculations. We compare our calculated spectra with the experimental ones [26, 28] and provide an interpretation of the key features seen in these spectra. The theoretical spectra are also compared with bulk h-BN, which has been studied in great detail before [19]. This comparison allows us to identify bonding effects between BN and the metal surfaces as well as effects related to the lattice mismatch in incommensurate structures.

2. Theoretical method

Density functional theory calculations were carried out using the WIEN2k [4] software package applying the full potential (FP) 'augmented-plane-wave + local orbitals' method (APW + lo) [18]. As exchange–correlation functional the generalized gradient approximation (GGA) by Wu–Cohen (WC) [36] was used. The equilibrium positions as given in [32, 15] were taken. The parameter determining the accuracy of the calculations, $R_{\mathrm{MT}} \cdot K_{\max}$ was set to 6.0, where R_{MT} is the smallest atomic sphere radius and $K_{\max}$ is the plane wave basis set cutoff. The atomic sphere radii for h-BN/Pt(111) and h-BN/Rh(111) were set to 1.35 au for boron and nitrogen, and 2.25 au for the metal atoms. In the case of the h-BN/Ni(111) interface, we used 1.32 au for B and N, and 2.11 au for the Ni atom. Since WIEN2k employs a 3D-periodicity (periodic boundary conditions), the interfaces are modeled by periodic slabs consisting of seven layers of metal covered by h-BN on both sides (in order to keep inversion symmetry which leads to real instead of complex matrix elements) and a vacuum region which extends to approximately 30 au. Since we also included core-hole effects in the simulations, the unit-cells of the interfaces were extended to 3×3 super-cells in the hexagonal plane in order to ensure sufficient screening of the introduced core hole [33] and to reduce the effects caused by the periodic images of the core hole. The Brillouin zone (BZ) was sampled with a $4\times4\times1$ mesh during the self-consistent-field procedure (SCF). Since the calculation of NEXAFS spectra requires an accurate density of states (DOS), we increased the mesh to $8 \times 8 \times 1$ for the spectra.

The theoretical spectra are calculated according to equation (1) and are proportional to the square of the dipole matrix elements between the core and conduction band wavefunctions, the corresponding partial DOS χ_l^{A} on atom A, and the energy conservation $\delta(\varepsilon - E_{\mathrm{core}}, h\nu)$

$$I(\nu) \propto \left|\left\langle \Psi^{\mathrm{cond}}_{A,l\pm1} \left| r \right| \Psi^{\mathrm{core}}_{A,n,l} \right\rangle\right|^2 \chi^{\mathrm{A}}_{l\pm1}(\varepsilon)\, \delta(\varepsilon - E_{\mathrm{core}}, h\nu)\,. \quad (1)$$

According to the dipole selection rule an absorption can only take place when the angular momentum quantum number l changes by 1, i.e. $\Delta l \pm 1$, between core and conduction band state. The presence of the core wavefunction in the dipole matrix element makes the absorption site specific and thus allows us to gather information about the chemical environment of the probed atom. According to the *final state rule* [33] the spectrum is predominantly determined by the electronic structure of the final state. In x-ray absorption the final state has a core hole but one additional electron in the conduction band. This situation can be considered as the static limit and represents the first approximation of the dynamical absorption process. Thus we can simulate the corresponding spectrum by supercell calculations, in which a core hole is introduced on one of the atoms (the probe atom). Therefore, for each calculated spectrum we have performed an independent SCF cycle. The conduction band states around this atom will feel a larger effective nuclear charge and thus will be attracted more strongly, where in the SCF calculation possible screening effects from the surrounding atoms are also included. In such a way, possible excitonic effects between core hole and conduction band electrons can be simulated quite accurately but in a fairly cheap way in contrast to the very expensive solutions of the Bethe–Salpeter equations (BSE), which furthermore can be applied only to insulating systems. It was shown by Olovsson *et al* [23] that in many cases the screening charge density of a supercell calculation agrees quite well with the corresponding exciton wavefunctions and consequently the simulated spectra are similar in the two approaches. However, one must admit that the quality of the core-hole screening depends on the size of the supercell (to avoid spurious hole–hole interactions) but also on the screening charge itself, i.e. the result depends on the state that the additional electron will actually occupy in the SCF procedure. It was shown, for example, by Moreau *et al* [19] that very good agreement can be obtained for the π^* states of BN (the low energy region) assuming a full core hole, whereas for the higher energy features a much smaller core hole is desirable, since the screening charge in π^* states cannot provide the correct screening for σ^* states. Experience has shown [30, 17, 11] that in many cases (except in very localized systems like wide bandgap insulators) a fractional core hole (e.g. only half a core hole) gives overall better results in accordance with Slater's transition state theory [35, 24] for excited states. The theoretical calculation cannot provide an absolute energy scale (the absolute core level energies will always have an error of a few electronvolt) and thus the theoretical spectra are aligned with the experimental spectra

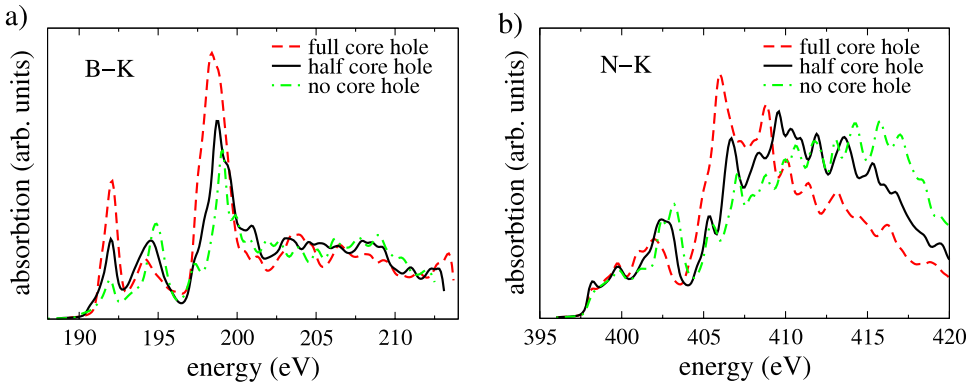

Figure 1. Theoretical B 1s (a) and N 1s (b) NEXAFS spectra for the h-BN/Ni(111) system. Calculations are carried out for no, 0.5, and a full core hole.

for best fit. It should be mentioned that the near-edge structure (ELNES) of electron energy loss spectra (EELS) can be also simulated in a very similar way, but in certain cases also higher multipole transitions need to be included. A fine review of EELS calculations using WIEN2k with lots of detail and examples was recently given by Hebert [11].

3. Results and discussion

3.1. h-BN/Ni(111)

The final state effects are included in our calculation of x-ray absorption spectra by introducing a core hole on our probe atom (a single selected N or B atom) within a large supercell. As mentioned above, its charge is, in principle, an undetermined quantity, which may vary between 0 e^- and 1 e^-. For the complicated h-BN/metal systems, an excited electron will NOT occupy the correct states, i.e. the B or N p bands, but in a core-hole simulation it will stay to a large extent in the metal d-bands. Therefore such simulations will not match the real process. For this reason we first investigate how much the size of the core hole influences the resulting spectra. We performed calculations in which the occupation of the 1s orbital of a single boron or nitrogen atom is decreased by 1, 0.5, or 0 while the number of valence electrons is increased accordingly. With such electronic configurations a self-consistent DFT calculation is carried out. At the final stage, the additional electron is removed from the valence panel in order to calculate the x-ray absorption spectra with the correct Fermi level. The resulting spectra are then broadened with a Gaussian and a Lorentzian of 0.35 eV. In figures 1(a) and (b) we present the B K and N K edge NEXAFS spectra calculated with zero, half, and a full core hole for the h-BN/Ni(111) system. One can immediately notice that the core hole shifts spectral weight from higher to lower energies. Such an effect is rather simple to understand, since the presence of a core hole increases the effective charge of the nucleus acting on the conduction electrons and due to the enhanced Coulomb interaction lowering the eigenenergies of the conduction band states. For the boron spectrum this leads mainly to a strong enhancement of the first peak (an excitonic like effect) and simultaneously a reduction of spectral weight of the second peak. For nitrogen the edge onset is much less sensitive to the core hole (the negative N ion screens the core hole much better). The fine structure of three peaks between 397 and 404 eV is visible in calculations with and without core hole. Later we will show that this spectral region is mainly determined by the hybridization between Ni-d and N p states and thus is less sensitive to excitonic effects. For the spectral features above 405 eV much larger core-hole effects are visible.

A comparison of the calculated spectra for boron and nitrogen with the experimental data [28] shows that all characteristic spectral features can be reasonably well reproduced by theory. For the B K spectrum the calculation without a core hole leads to results with a completely wrong ratio in intensities between first and second peaks. In a calculation with a full core hole, the energies of the transitions in the B K spectra are well reproduced but the intensity of the third peak (about 198 eV) is overestimated in comparison with the second peak. The intermediate case with half a core hole overestimates the intensity of the second peak, but agrees better with experiment for the third one and thus we compare this calculation with experiment in figure 2. In the case of the N K spectra, the effects are less distinctive than for B, but also here the calculation with half a core hole gives the best agreement. The spectrum derived with a full core hole leads to the worst agreement, since the peak at 406 eV is too intensive. As a compromise we use half a core hole in all further calculations.

The NEXAFS spectra reflect the structure of the unoccupied electronic states. The difference between the spectra of the h-BN/metal interface and those of bulk h-BN show how the conduction bands are modified by the interaction between h-BN and the metal surface. The comparison of calculated B K and N K spectra for h-BN/Ni(111) and bulk h-BN is presented in figure 3. For both cases the comparison shows distinct similarities and differences. The B K edge of bulk h-BN shows only two pronounced features in the investigated energy range: a very sharp and narrow peak at 192 eV and a broader feature around 198 eV. The occupied part of the electronic structure of h-BN consists of bonding N–B sp^2-σ bands and p_z-π bands, while the unoccupied part is formed by antibonding π^* and σ^* bands. The corresponding B and N p DOS can be seen in figure 4. The sharp first peak

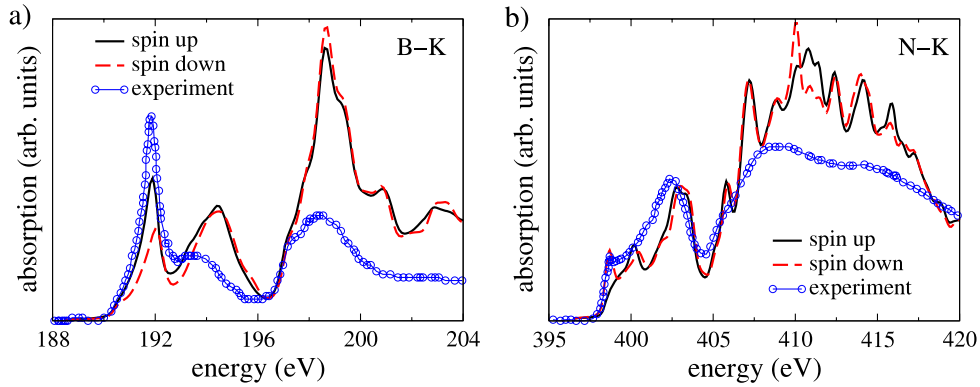

Figure 2. B 1s (a) and N 1s (b) NEXAFS spectra for the h-BN/Ni(111) system. Theoretical results are obtained with 0.5 core holes (solid and dashed lines) and experimental data (open circles) are from [28].

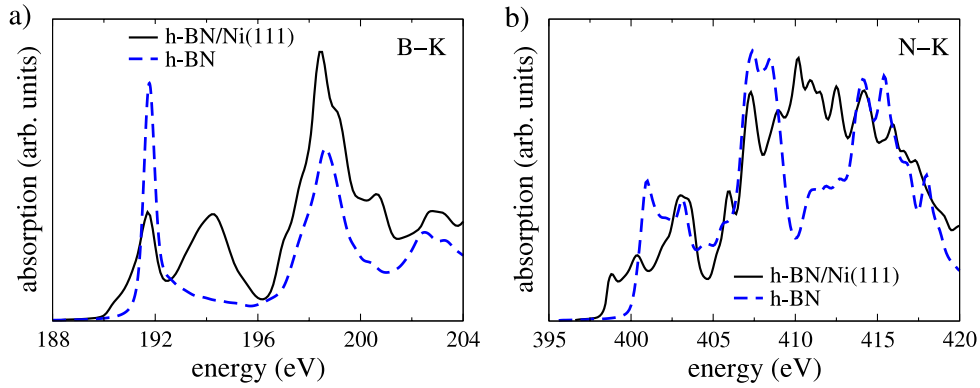

Figure 3. Comparison of calculated B 1s (a) and N 1s (b) NEXAFS spectra for h-BN/Ni(111) and bulk h-BN.

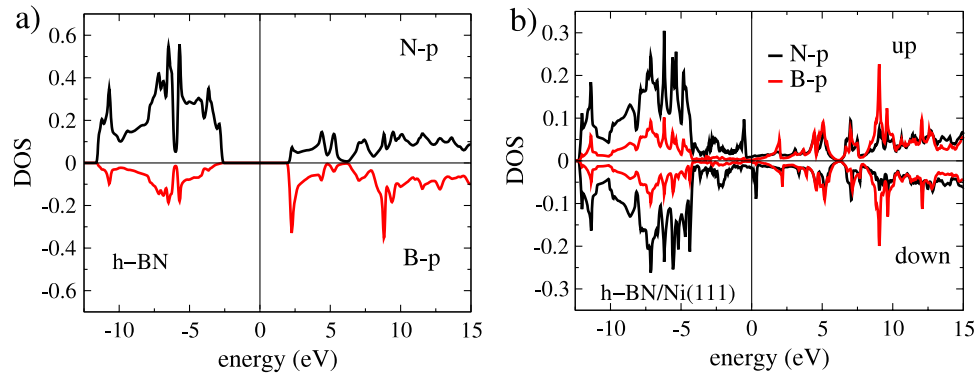

Figure 4. B p and N p DOS for (a) bulk h-BN, (b) h-BN/Ni(111) interface.

in the B K spectrum corresponds to transition into the π^* band and became so sharp due to excitonic effects. The second peak is mainly due to transitions into the σ^* band and shows much weaker core-hole effects. The B K spectrum of h-BN/Ni(111) has a much wider first peak with a small shoulder on the left side due to a small spin-splitting caused by the interactions with Ni, and a new peak around 194 eV develops. A comparison of the corresponding DOS (figure 4) explains these features, which come from the distinct interaction between h-BN and the Ni-surface. The N K edge of bulk h-BN shows three double peaks centered at 402, 408, and 415 eV with a sharp onset at 400 eV. The h-BN/Ni(111) interface shows only a broad absorption at higher energies, but in particular forms a so-called 'pre-peak' just below 400 eV. This feature has previously been found by Preobrajenski *et al* [28] in the measured spectra. In order to understand the origin of the pre-peak we look again at the projected N p DOS (figure 4). The main features of the bulk h-BN DOS are still present in the h-BN/Ni(111) interface, but the gap between bonding and antibonding states has been filled in particular by N-p_z states due to a strong interaction with the metal d-band, as discussed in detail in [15]. The Ni-d_{z^2} DOS (not shown here)

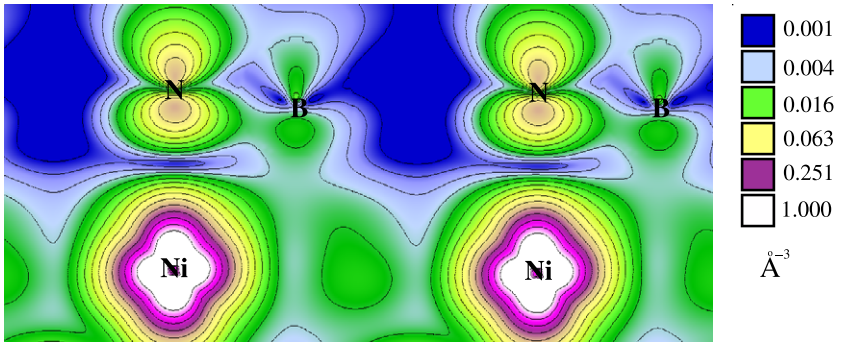

Figure 5. Electron density for spin-down states within an energy range of 0–0.75 eV (exponential scaling).

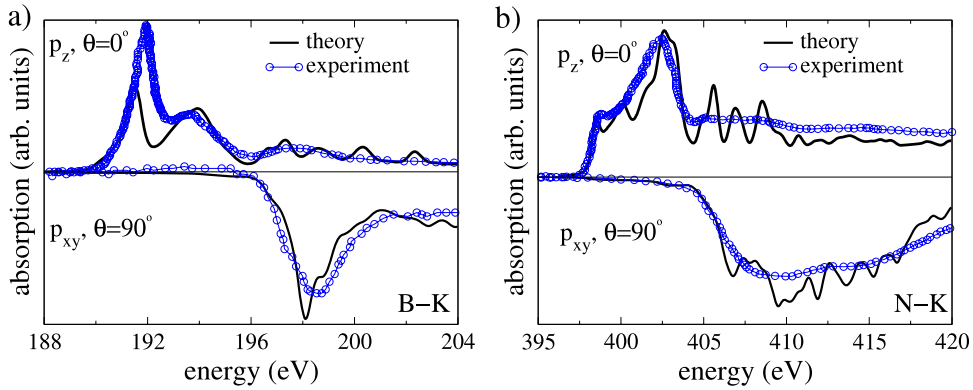

Figure 6. Angular dependent B 1s (a) and N 1s(b) NEXAFS spectra calculated for the h-BN/Ni(111) system. Calculations were performed for $\Theta = 0°$ and 90° with 0.5 core holes (solid line) and are compared to experimental data (open circles) for $\Theta = 20°$ and 90° from [26].

shows a distinct spin-split peak just below and above the Fermi energy. The hybridization with N-p_z states is clearly evident in figure 4(b) and the peak just above the Fermi level constitutes the pre-peak feature in the N K edge. The spin-resolved N K spectra (see figure 2) show the 'pre-peak' only in the spin-down channel. In figure 5 we plot the charge density calculated from states in a narrow energy window covering this peak. The relatively low charge density with a narrow minimum between the Ni and N atoms shows that these states can be characterized as antibonding N-p_z–Ni-d_{z^2} hybrids.

In principle, experimental spectra of oriented single crystalline samples can be measured with a different geometrical setup. The angular dependence of spectral features provides additional valuable information about the nature and character of the probed electronic states. Many measurements of B K and N K edges have been performed [19, 26, 34, 8, 25, 31, 16, 7, 2, 27] and the measured intensities are very sensitive to the small experimental details, especially the angle of incidence and the filtering methods.

In order to analyze such effects, we calculated B K and N K spectra for h-BN/Ni(111) using the corresponding projected p_z and $p_{x,y}$ DOS instead of the total p DOS as before. Such calculations correspond to measurements with 0° and 90° for the angle of incidence, respectively. Since it is not possible to do measurements with an incident angle of 0°, the calculated spectra are compared to measured spectra for 20° [26]. The calculated and measured spectra are compared in figure 6 for boron and nitrogen and the theoretical results perfectly match the experiments. Obviously for both B K and N K spectra the intensities at low energies originate only from transitions to p_z orbitals, while the broad peaks at higher energies are related mainly to transitions into $p_{x,y}$ states. This can be well understood by the analysis given above, where we have shown that the antibonding π^* bands are lower in energy and well separated from the σ^* bands.

3.2. h-BN/Pt(111), h-BN/Rh(111)

The theoretical analysis of the incommensurate h-BN/metal interfaces (nanomeshes) is much more difficult than for h-BN/Ni(111) due to the huge size of the unit-cell. For example, the h-BN/Rh(111) structure consists of a coincidence lattice of 13 × 13 h-BN and 12 × 12 Rh(111) unit-cells. The *ab initio* calculations reported so far have been performed for slabs with only three metal layers [13], but already this thin slab contains 1108 atoms in the simulation box and thus requires an extremely large computational effort. Therefore, it is not feasible to perform separate core-hole calculations for all 338 inequivalent B and N atoms. In order to analyze the spectra of such a complicated system we must approximate the real structures by small commensurate 1 × 1 unit-cells. While in principle all 338 B and N atoms are different because they have slightly different (lateral) positions with respect to the metal surface, the BN atoms of the nanomesh can in a first approximation be split into two different but representative

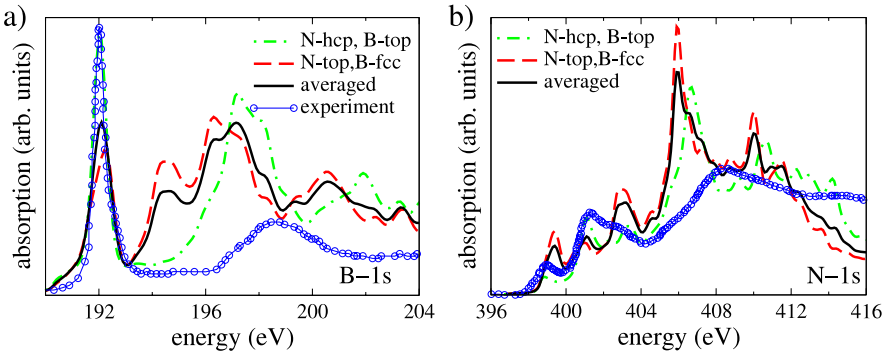

Figure 7. (a) B 1s, (b) N 1s NEXAFS spectra for h-BN/Rh(111). Calculations carried out using 0.5 core holes in comparison to experimental data (circles) [28]. Both bonding (N-top, B-fcc) and non-bonding (N-hcp, B-top) configurations are shown, as well as their weighted average (0.7:0.3).

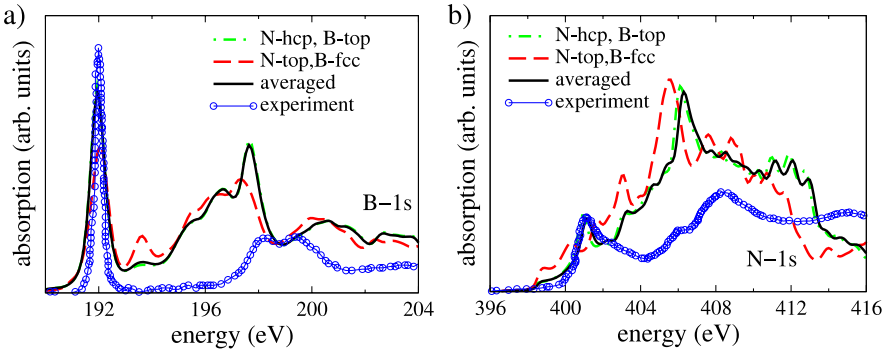

Figure 8. (a) B 1s, (b) N 1s NEXAFS spectra for h-BN/Pt(111). Calculations carried out using 0.5 core holes in comparison to experimental data (circles) [28]. Both bonding (N-top, B-fcc) and non-bonding (N-hcp, B-top) configurations are shown, as well as their weighted average (0.1:0.9).

regions, namely into those of the pores (holes) and on the wires (see [14]). In the first region (pores), where the h-BN atoms are attracted to the metal surface (bonding region), the BN atoms are close to a (N-top, B-fcc) configuration and thus stay close to the metal surface (2.2 and 2.3 Å for Rh and Pt, respectively). On the wires, however, the h-BN atoms are repelled from the metal surface and, for instance, in the h-BN/Rh(111) nanomesh the BN atoms are about 0.6 Å further away from the metal surface. In this region the BN atoms are close to (N-hcp, B-top) and (N-hcp, B-fcc) sites [14]. The electronic structure of h-BN is different in these two regions, in particular the specific metal-B and metal-N interactions or the N–B-metal charge transfer differs significantly. Therefore, we will approximate the spectra of the nanomeshes by an area-weighted superposition of two distinct 1×1 cell calculations with h-BN in the (N-top, B-fcc) and (N-hcp, B-top) position, located at the corresponding equilibrium distance from the metal surface, respectively. This approximation results in a stretching of h-BN to the unit-cell size of the metal surface and, as will be discussed below, will have an effect on the position of the antibonding σ^* bands with respect to the π^* bands, which are much less affected by this stretching.

The results for h-BN/Rh(111) and for h-BN/Pt(111) are presented in figures 7 and 8, respectively. We immediately notice that for all cases the positions of the higher energy peaks in the calculated spectra are shifted towards lower energies by about 2 eV relative to the position in the experimental spectra [28]. This is a direct consequence of the stretching of the h-BN bonds and thus the reduced σ–σ^* bonding–antibonding splitting. The same shift is observed when we compare the spectra calculated for bulk h-BN with stretched and equilibrium unit-cell parameters. We see for both cases, Rh and Pt, that the spectra depend rather strongly on the h-BN position (height and lateral). The bonding configuration (N-top, B-fcc) results in spectra that are quite similar to the one we observed for the Ni case, whereas the spectra for the non-bonding position (N-hcp, B-top) are much closer to the bulk h-BN results. For the B K edges the peak at 194 eV is observed only for (N-top, B-fcc) configurations. This feature is much more pronounced for the Rh(111) than for the Pt(111) surface, because there is a much stronger bonding between h-BN and Rh(111) than to Pt(111) [15]. The B K spectra of these two interfaces for the non-bonding configuration are similar to each other. The experimental B K spectra measured by Preobrajenski [28] seem to be very close to the results of the non-bonding configurations, when we consider the correction due to stretching. But note that the measured spectra have a distinct orientational sensitivity and the strength of the 194 eV B K edge feature depends on the experimental setup [27]. Eventually, a 'full core hole' calculation, which is more appropriate for π^*-bands, would further reduce the 194 eV peak and enhance the agreement with the experiment.

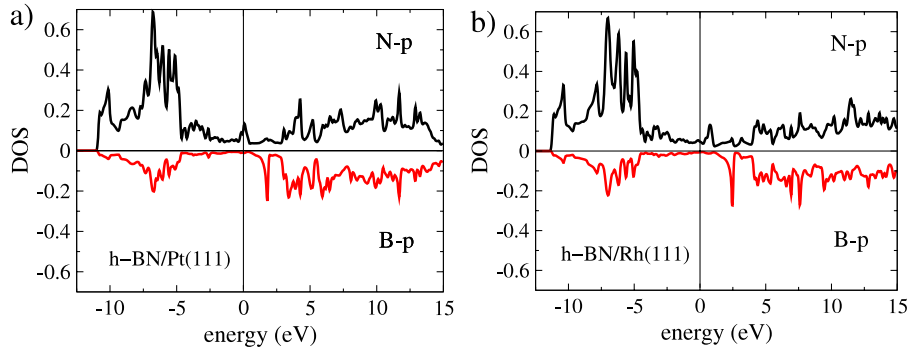

Figure 9. B p and N p DOS for (a) h-BN/Pt(111) interface, (b) h-BN/Rh(111) interface calculated for the bonding (N-top, B-fcc) configuration.

The N K spectrum of h-BN/Rh(111) for the bonding (N-top, B-fcc) configuration shows the so-called 'pre-peak', which is not present either for Pt(111) or in the non-bonding configurations. As discussed for the Ni(111) interface, the 'pre-peak' originates from the antibonding N-metal states forming a sharp DOS peak around the Fermi level (see DOS in figure 9). For Rh(111) this DOS peak is well above the Fermi level because Rh has a smaller number of d electrons, whereas in the Pt(111) case with an almost full d-band it is partly below the Fermi level. Comparing the onset of the calculated N K spectra with experiment we noticed that relatively good agreement can be reached by averaging the spectra of the bonding and non-bonding regions with a weight proportional to the area of the corresponding regions. For the h-BN/Rh(111) nanomesh, the large pores lead to a fraction of 70% bonding and 30% non-bonding regions, while for the 'Moiré'-pattern of h-BN/Pt(111) only a 10% bonding region is present (figures 7 and 8).

4. Conclusions

We have presented calculations of B K and N K NEXAFS spectra for three different h-BN/metal interfaces: h-BN/Ni(111), h-BN/Rh(111), and h-BN/Pt(111). The h-BN/Ni(111) interface has a simple commensurate 1×1 structure, whereas the other two form more complicated, so-called nanomesh structures, where (due to an approximate coincidence lattice of h-BN and the metal surface) several topologically different configurations of h-BN relative to the metal surface coexist. From another point of view these interfaces differ also in the interaction strength between h-BN and the metal: the h-BN/Ni(111)and h-BN/Rh(111) interfaces show strong h-BN to metal interactions, while h-BN is relatively weakly bonded to Pt(111).

We have discussed in detail the final state effects and argued that for such metallic interfaces the screening charge cannot be placed into the correct states (B and N p bands), but will occupy metal d-bands. Therefore a full core hole on B or N atoms, might not be properly screened by its corresponding conduction electron. The fractional core hole used in this work can sometimes correct such insufficient screening. In the case of the h-BN/Ni(111) interface we tested the influence of the size of the core hole on the spectra and we showed that half a core hole results in the relatively best agreement with the measured spectra, although for the low energy spectra a full core hole would be preferable.

For strongly bonded interfaces, both N K and B K spectra show strong features related to the interaction between h-BN and the metal. In the case of B K it is the presence of the peak at 194 eV. The height of this peak is very sensitive to the interaction between h-BN and the metal surface, but also core-hole effects are essential. For N K spectra the h-BN metal interaction results in the formation of the so-called 'pre-peak'. We show that such 'pre-peaks' occur due to a peak in the DOS stemming from an antibonding N-p_z–metal-d_{z^2} interaction. In the case of Pt(111) such a peak does not appear in the spectra, because the interaction is much weaker and the corresponding peak appears mostly in the occupied part of the DOS and thus is not visible in XAS. For Ni(111) and Rh(111) these states form relatively sharp DOS peaks above the Fermi level. The 'pre-peak' is not present in the spectra calculated for non-bonding configurations of Rh(111) and Pt(111) interfaces.

Overall our calculations explain all experimentally detected spectral features, but the quantitative agreement is sometimes not perfect due to final state effects and structural approximations necessary to model the nanomesh systems.

References

[1] Auwärter W, Kreutz T J, Greber T and Osterwalder J 1999 *Surf. Sci.* **429** 229–36
[2] Barth J, Kunz C and Zimkina T M 1980 *Solid State Commun.* **36** 453
[3] Berner S, Corso M, Widmer R, Groening O, Laskowski R, Blaha P, Schwarz K, Goriachko A, Over H, Gsell S, Schreck M, Sachdev H, Greber T and Osterwalder J 2007 *Angew. Chem. Int. Edn Engl.* **46** 5115
[4] Blaha P, Schwarz K, Madsen G K H, Kvasnicka D and Luitz J 2001 *WIEN2k, An Augmented Plane Wave Plus Local Orbitals Program for Calculating Crystal Properties* Vienna University of Technology Austria, ISBN 3-9501031-1-2
[5] Corso M, Auwärter W, Muntwiler M, Tamai A, Greber T and Osterwalder J 2004 *Science* **303** 217
[6] Corso M, Greber T and Osterwalder J 2005 *Surf. Sci.* **577** L78
[7] Franke R, Bender S, Hormes J, Pavlychev A A and Fominych N G 1997 *Chem. Phys.* **216** 243

[8] Fuentes G G, Borowiak-Palen E, Pichler T, Liu X, Graff A, Behr G, Kalenczuk R J, Knupfer M and Fink J 2003 *Phys. Rev.* B **67** 035429
[9] Goriachko A, He Y, Knapp M, Over H, Corso M, Brugger T, Berner S, Osterwalder J and Greber T 2007 *Langmuir* **23** 2928
[10] Grad G B, Blaha P and Schwarz K 2003 *Phys. Rev.* B **68** 085404
[11] Hebert C 2007 *Micron* **38** 12
[12] Huda M N and Kleinman L 2006 *Phys. Rev.* B **74** 75418
[13] Laskowski R and Blaha P 2008 *J. Phys.: Condens. Matter* **20** 064207
[14] Laskowski R, Blaha P, Gallauner T and Schwarz K 2007 *Phys. Rev. Lett.* **98** 106802
[15] Laskowski R, Blaha P and Schwarz K 2008 *Phys. Rev.* B **78** 045409
[16] Li D, Bancroft G M and Fleet M E 1996 *J. Electron Spectrosc. Relat. Phenom.* **79** 71
[17] Luitz J, Maier M, Hebert C, Schattschneider P, Blaha P, Schwarz K and Jouffrey B 2001 *Eur. Phys. J.* B **21** 363
[18] Madsen G K H, Blaha P, Schwarz K, Sjöstedt E and Nordström L 2001 *Phys. Rev.* B **64** 195134
[19] Moreau P, Boucher F, Goglio G, Foy D, Mauchamp V and Ovrard G 2006 *Phys. Rev.* B **73** 195111
[20] Morscher M, Corso M, Greber T and Osterwalder J 2006 *Surf. Sci.* **600** 3280
[21] Nagashima A, Tejima N, Gamou Y, Kawai T and Oshima C 1995 *Phys. Rev.* B **51** 4606
[22] Nagashima A, Tejima N, Gamou Y, Kawai T and Oshima C 1995 *Phys. Rev.* B **51** 4606–13
[23] Olovsson W, Tanaka I, Puschnig P and Ambrosch-Draxl C 2008 *AMTC Lett.* **1** 136
[24] Perdew J P and Zunger A 1981 *Phys. Rev.* B **23** 5048–79
[25] Pettifer R F, Brouder C, Benfatto M, Natoli C R, Hermes C and Ruiz Lopez M F 1990 *Phys. Rev.* B **42** 37–42
[26] Preobrajenski A B, Vinogradov A S and Mårtensson N 2004 *Phys. Rev.* B **70** 165404
[27] Preobrajenski A B, Vinogradov A S and Mårtensson N 2005 *Surf. Sci.* **582** 21
[28] Preobrajenski A B, Vinogradov A S, Ng M L, Ćavar E E, Westerström R, Mikkelsen A, Lundgren E and Mårtensson N 2007 *Phys. Rev.* B **75** 245412
[29] Shimoyama I, Baba Y, Sekiguchi T and Nath K G 2004 *J. Electron Spectrosc. Relat. Phenom.* **137** 573–8
[30] Strocov V N, Schmitt T, Rubensson J E, Blaha P, Paskova T and Nilsson P O 2005 *Phys. Rev.* B **72** 85221
[31] Terminello L J, Chaiken A, Lapiano-Smith D A, Doll G L and Sato T 1994 *J. Vac. Sci. Technol.* A **12** 2462
[32] Tran F, Laskowski R, Blaha P and Schwarz K 2007 *Phys. Rev.* B **75** 115131
[33] von Barth U and Grossmann G 1982 *Phys. Rev.* B **25** 5150–79
[34] Widmayer P, Boyen H-G, Ziemann P, Reinke P and Oelhafen P 1999 *Phys. Rev.* B **59** 5233
[35] Williams A R and deGroot R A 1975 *J. Chem. Phys.* **63** 628–31
[36] Wu Z and Cohen R E 2006 *Phys. Rev.* B **73** 235116